RSC Advances

PAPER

View Article Online
View Journal | View Issue

Check for updates

Cite this: *RSC Adv.*, 2025, **15**, 28827

Photoluminescent phenanthroimidazole derivatives as covalently linked UV stabilizers for latex coatings

Liudmila Loghina, *[a] Jana Machotova,[b] Roman Svoboda,[b] Jakub Houdek,[a] Miroslav Kohl,[b] Zdena Ruzickova,[c] Roman Jambor [c] and Miroslav Vlcek [ac]

Synthetic latexes are widely used as binders for outdoor barrier applications, where ultraviolet (UV) protection is of high practical importance. This study reports the synthesis of two novel, highly photoluminescent phenanthroimidazole (PPI) derivatives and their application as covalently linked UV-absorbing stabilizers in waterborne, photostable coatings based on all-acrylic latex polymers. Vinyl-functionalized phenanthroimidazole-based monomers, namely 1,2-bis(4′-vinyl-[1,1′-biphenyl]-4-yl)-1*H*-phenanthro[9,10-*d*]imidazole (**DV-bPPI**) and 1,2-bis(4-vinylphenyl)-1*H*-phenanthro[9,10-*d*]imidazole (**DV-PPI**), were synthesized *via* Suzuki cross-coupling with high yield up to 85%. The synthesized monomers were characterized by multinuclear NMR, FTIR spectroscopy, and single-crystal X-ray diffraction analysis. PPI derivatives, in amounts ranging from 0.05 to 1 wt% (based on monomers), were copolymerized with methyl methacrylate, butyl acrylate, and methacrylic acid using a standard emulsion polymerization technique. The resulting coatings were fully transparent in the visible region and were characterized by UV-vis and photoluminescence measurements. Dynamic mechanical analysis demonstrated that **DV-bPPI** and **DV-PPI**, at concentrations of 0.5–1 wt% and 0.25–0.5 wt%, respectively, effectively prevented UV-induced degradation of the polymer films.

Received 16th July 2025
Accepted 7th August 2025

DOI: 10.1039/d5ra05109f

rsc.li/rsc-advances

Open Access Article. Published on 13 August 2025. Downloaded on 8/22/2025 11:09:28 PM.
This article is licensed under a Creative Commons Attribution-NonCommercial 3.0 Unported Licence.

Introduction

The coatings industry is transforming profoundly, with waterborne coatings replacing solvent-based products due to environmental pressure and increased customer preferences. An ecologically-friendly nature is required not only for final products but also for technological synthesis processes. For this reason, latexes, *i.e.*, aqueous polymer dispersions produced by emulsion polymerization, are a popular group of synthetic materials with increasing worldwide production. In the standard emulsion polymerization technology, unsaturated monomers are dispersed in the aqueous continuous phase using surfactants and transformed by radical polymerization into polymer particles with a typical size of 50–200 nm.[1,2]

Synthetic latexes are widely used in the building and construction industries as binders for barrier and protective coating systems. Durability and longevity remain critical performance properties for these materials. In the case of exterior applications, this requirement usually means preventing the photodegradation of polymer upon exposure to ultraviolet (UV) light. Various methods are used for this purpose, among which the all-acrylic latex binders (a class of polymers that are considered highly UV-resistant),[3,4] inorganic nanomaterials,[5,6] and organic UV-absorbing stabilizers are frequently used for the fabrication of clearcoats and non-pigmented latex protective coatings.[7,8]

Organic UV absorbers (UVAs) are compounds transparent for all visible light ($\lambda > 400$ nm), that exhibit high UV-radiation ($\lambda \leq 400$ nm) absorbance rates followed by conversion of all excitation energy into less harmful energy (visible light or heat), thereby protecting the polymer and/or the underlying substrate from degradation.[9,10] Currently, there are multiple requirements for UV absorbers, and long-term protection is the most significant among them. Therefore, these compounds should not degrade in the long term, evaporate from the polymer matrix, be leached out by solvents, or be removed in any other way. Furthermore, effective UV-absorbing stabilizers must be uniformly distributed, which requires compatibility with the polymer. Several approaches have been developed to overcome these risks, where the chemical anchoring to the polymer backbone is a possible solution. The most promising compounds appear to be those containing heterocyclic donor- and donor–acceptor fragments. Recently, the ability to absorb UV radiation has been demonstrated in such organic UV

[a]*Center of Materials and Nanotechnologies, Faculty of Chemical Technology, University of Pardubice, 53002 Pardubice, Czech Republic. E-mail: Liudmila.Loghina@upce.cz*

[b]*Institute of Chemistry and Technology of Macromolecular Materials, Faculty of Chemical Technology, University of Pardubice, 53210 Pardubice, Czech Republic*

[c]*Department of General and Inorganic Chemistry, Faculty of Chemical Technology, University of Pardubice, 53210 Pardubice, Czech Republic*

© 2025 The Author(s). Published by the Royal Society of Chemistry

Open Access Article. Published on 13 August 2025. Downloaded on 8/22/2025 11:09:28 PM. This article is licensed under a Creative Commons Attribution-NonCommercial 3.0 Unported Licence.

absorbers as benzotriazoles,[11] triazines,[12] malonates, and hindered amines.[13] Functionalization of already known and new organic photoluminescent compounds using vinyl or allyl groups can ensure their chemical incorporation into the polymer chain *via* radical polymerization. They can act here as a UV absorber that is resistant to migration and eventual washing out of the polymer material.[14]

In this research, we focused on highly photostable waterborne coatings based on all-acrylic latex polymer with chemically anchored UVA. Therefore, we investigated the possibility of introducing another group of UV-absorbing compounds into the polymer. This group is represented by two novel PPI derivatives prepared by functionalizing already-known compounds[15–19] with a vinyl bond. Phenanthroimidazole-based compounds 1,2-bis(4′-vinyl-[1,1′-biphenyl]-4-yl)-1*H*-phenanthro[9,10-*d*]imidazole (**DV-bPPI**) and 1,2-bis(4-vinylphenyl)-1*H*-phenanthro[9,10-*d*]imidazole (**DV-PPI**) were successfully vinyl-functionalized by Suzuki cross-coupling reaction and characterized by multinuclear NMR, FTIR, and single-crystal X-ray diffraction analysis. Two novel PPI-based UVAs (absorbance region 250–400 nm) with vinyl groups were copolymerized with acrylic monomers *via* emulsion polymerization. In clearcoats, UVAs are typically used at 3 wt% based on the solids.[20] In this work, lower UVA concentrations (0.05–1 wt%) were utilized, and the effects of UVA type and concentration on UV stabilizing efficiency were investigated according to changes in chemical structure, glass transition temperature (T_g), and thermo-mechanical properties of the non-exposed and UV-exposed films.

Experimental section

Materials and methods

4-Bromobenzaldehyde, phenanthrene-9,10-dione, 4-bromoaniline, vinylboronic acid pinacol ester, purchased from BLD Pharmatech GmbH, (4-vinylphenyl)boronic acid from TCI Europe, and Disponil FES 993 from BASF (Germany) were used as received. Acrylic monomers, ammonium persulfate, sodium carbonate, glacial acetic acid, ammonium acetate, and solvents were purchased from Fisher Scientific and used as delivered.

The Nuclear Magnetic Resonance (NMR) spectra were recorded from solutions in $CDCl_3$ at 295 K on a Bruker AscendTM 500 spectrometer (equipped with Z-gradient 5 mm Prodigy cryoprobe) at frequencies 500.13 MHz for ^{1}H and 125.76 MHz for ^{13}C correspondingly. The solutions were obtained by dissolving approximately 50 mg of each compound in 1.0 ml of $CDCl_3$. The values of ^{1}H chemical shifts were calibrated to residual signals of $CDCl_3$ (δ (1H) = 7.26 ppm). The values of ^{13}C chemical shifts were referenced to the signals of $CDCl_3$ (δ (^{13}C) = 77.23 ppm). Positive chemical shift values denote shifts to the higher frequencies relative to the standards. IR spectra in the region 4500–500 cm^{-1} (resolution of 2 cm^{-1}) were measured using a single-bounce diamond ATR crystal on a Vertex 70 V FT-IR spectrometer (Bruker, Germany).

Diffraction data for **DV-bPPI** (2) and **DV-PPI** (3) were collected using a Bruker Venture D8 diffractometer (Bruker, Germany) at 150 K with graphite-monochromated Mo-Kα (0.7107 Å) radiation. The frames were integrated with the Bruker SAINT software package using a narrow frame algorithm. Data were corrected for absorbance effects using the multi-scan method (SADABS). The obtained data were treated by the XT version 2014/5 and SHELXL-2019/1 software implemented in APEX4 v2021.10-0 (Bruker AXS) system. All non-hydrogen atoms were refined using anisotropic displacement parameters. Crystallographic data for the structural analyses have been deposited with the Cambridge Crystallographic Data Centre, CCDC nos. 2414305 and 2414306. Copies of this information may be obtained free of charge from The Director, CCDC, 12 Union Road, Cambridge CB2 1EZ, UK (Fax: +44-1223-336033; e-mail: deposit@ccdc.cam.ac.uk or **http://www.ccdc.cam.ac.uk**). Elemental analyses were performed on a LECO-CHNS-932 analyser.

The latex synthesis characteristics from the point of view of the coagulum content and overall monomer conversion were determined according to standard procedures.[21] After the synthesis, the latexes were characterized regarding the average hydrodynamic diameter and zeta potential values of polymer particles using dynamic light scattering (DLS) with a Litesizer 500 instrument (Anton Paar GmbH, Austria). The measurements were performed at a solid polymer concentration of 0.01 wt% in the water phase and at 25 °C.

The visual assessment of the latex film's macroscopic and microscopic appearance was carried out using a calibrated adjustable Dino-Lite Edge 3.0 (AnMo Electronics Corporation, New Taipei City, Taiwan) microscopic probe and an optical microscope Olympus BX51 with the VIS SenTech MC83 camera (combined with a ×10 objective; reflection mode). The structural/chemical morphology was also investigated on the micro-scale employing Raman microscopy, using a DXR2 Nicolet Raman microscope (ThermoFisher Scientific, USA), utilizing the 785 nm excitation diode laser (30 mW, laser spot size 3.1 μm) and a CCD detector. The standard setup for the collection of the Raman signal was as follows: a laser intensity of 20 mW, a single scan duration of 3s, 50 scans per Raman spectrum.

The T_g of dried latex polymer films was determined by differential scanning calorimetry (DSC), using a heat-flow DSC Q2000 instrument (TA Instruments, USA) equipped with an autosampler, RCS90 cooling accessory, and T-zero technology. The DSC was calibrated based on the melting temperatures and enthalpies of the In, Zn, and H_2O standards. For the DSC measurements, discs with a diameter of 4 mm were cut from the latex film (their masses varied between 10–30 mg) and inserted in open low-mass T-zero Al pans (the measurements were performed in a static air atmosphere). During simple heating from −40 to 60 °C at 5 °C min^{-1}, a single glass transition effect (characterized by the distinct T_g) occurred; the corresponding T_g was evaluated as a half-height midpoint.

The gel content of latex polymers was evaluated following the CSN EN ISO 6427 standard based on the Soxhlet extraction using tetrahydrofuran (THF).

Specimens in the form of 4 mm diameter discs cut from dry latex films were also used for testing the thermo-mechanical properties by dynamic mechanical analysis (DMA). The DMA 303 Eplexor instrument (Netzsch, Germany) was used in the penetration mode (cylindrical pin with a diameter of 1 mm); the

 © 2025 The Author(s). Published by the Royal Society of Chemistry

Open Access Article. Published on 13 August 2025. Downloaded on 8/22/2025 11:09:28 PM. This article is licensed under a Creative Commons Attribution-NonCommercial 3.0 Unported Licence.

point of contact was in the middle of the top base of the latex film disc. The measurements of the as-prepared latex films were performed with a sinusoidal dynamic load frequency of 1 Hz, constant dynamic displacement of 5 μm (dynamic force limit of 3 N), proportional factor between static and dynamic load $F_{stat}/F_{dyn} = 1.3$, and static strain limit of 100%; for the UV-irradiated films, the dynamic force limit was set to 5 N. The measurements were performed in the temperature range from −30 to 40 °C at 5 °C min^{-1}. The moduli were calculated for the cylindrical geometry characterized by the height of the latex disc and the contact area with the penetration probe (0.785 mm^2).

The accelerated UV weathering of dry latex polymer films was done in a QUV/se Tester (Q-Panel Lab Products, USA) using fluorescent tubes UVA-340 (having a maximum emission at a wavelength of 340 nm). The weathering procedure was set as follows: 0.89 W m^{-2} at 340 nm, temperature of 60 ± 2 °C, relative humidity of 50 ± 5%, and 720 h (30 days) of continuous irradiation [https://www.doi.org/10.1016/0300-9440(94)00525-7].

The optical properties were measured using a Fluorometer PTI QuantaMaster 400 (Horiba, Germany) to obtain PL data in the spectral range of 300–850 nm using excitation wavelength λ = 300–500 nm and a UV-3600 (Shimadzu, Japan) spectrometer to get UV-vis absorbance spectra in the spectral range 200–800 nm.

Synthetic procedure

1,2-Bis(4-bromophenyl)-1*H*-phenanthro[9,10-*d*]imidazole (2-Br-PPI) (1). To a mixture of 4-bromobenzaldehyde (5.0 g, 0.027 mol) and phenanthrene-9,10-dione (5.62 g, 0.027 mol) in 120 ml of glacial acetic acid were added successively 4-bromoaniline (9.29 g, 0.054 mol) and ammonium acetate (6.24 g, 0.081 mol) with permanent stirring. The reaction mixture was stirred under reflux for 7 h. The conversion of the product was monitored by TLC (CH_2Cl_2). The cooled reaction mixture was diluted 3 times with water, the precipitate was filtered off and washed on the filter several times with water, then with ethanol. After drying in air, the product was purified by flash column chromatography (CH_2Cl_2) to give a pure product. White-off powder; yield: 12.37 g (86.7%). Anal. calcd for $C_{27}H_{16}Br_2N_2$ (M_r = 528.25): C, 61.39%; H, 3.05%; Br, 30.25%; N, 5.30%. Found: C, 61.59%; H, 2.99%; Br, 29.72%; N, 5.19%. ^{1}H NMR (500.13 MHz, $CDCl_3$), δ: 8.83 (dd, $^3J_{H,H}$ = 8.0 Hz, $^4J_{H,H}$ = 1.0 Hz, 1H^1), 8.76 (d, $^3J_{H,H}$ = 8.4 Hz, 1H^8), 8.69 (d, $^3J_{H,H}$ = 8.4 Hz, 1H^5), 7.76–7.72 (m, 3H$^{6,\ 10}$), 7.66 (ddd, $^3J_{H,H}$ = 8.4, 6.9 Hz, $^4J_{H,H}$ = 1.2 Hz, 1H^7), 7.53 (ddd, $^3J_{H,H}$ = 8.3, 6.9 Hz, $^4J_{H,H}$ = 1.1 Hz, 1H^2), 7.45 (dt, $^3J_{H,H}$ = 10.6, 2.1 Hz, 2H^{12}), 7.40 (dt, $^3J_{H,H}$ = 10.6, 2.0 Hz, 2H^9), 7.35 (dt, $^3J_{H,H}$ = 11.0, 2.6 Hz, 2H^{11}), 7.2 (ddd, $^3J_{H,H}$ = 8.1, 6.9 Hz, $^4J_{H,H}$ = 0.8 Hz, 1H^3), 7.19 (d, $^3J_{H,H}$ = 8.3 Hz, 1H^4). ^{13}C NMR (125.76 MHz, $CDCl_3$), δ: 149.85 (N–C=N), 137.73, 133.73, 131.78, 130.99, 130.77, 129.55, 129.30, 128.49, 128.20, 127.60, 127.15, 126.66, 126.07, 125.39, 124.43, 124.21, 123.77, 123.33, 122.87, 122.85, 120.81. IR (ATR, cm^{-1}) 3056 ν (CH_{aryl}); 1607 ν (C=CN), 1489 ν ($C=C_{aryl}$); 831 Υ ($C–H_{aryl}$).

1,2-Bis(4′-vinyl-[1,1′-biphenyl]-4-yl)-1*H*-phenanthro[9,10-*d*] imidazole (DV-bPPI) (2). **2-Br-PPI** (1) (5.28 g, 10 mmol), 2 M K_2CO_3 (20 ml), ethanol (50 ml), and 100 ml of toluene were mixed in a three-necked flask under vigorous stirring. The mixture was degassed by replacing air with argon. (4-Vinylphenyl)boronic acid (3.10 g, 21 mmol) and tetrakis(triphenylphosphine)palladium(0) (0.73 g, 0.63 mmol) were added. After repeated degassing, the reaction mixture was stirred under reflux in a slow stream of argon for 5 h. TLC control (CH_2Cl_2). Then, the mixture was quenched with water (50 ml) and extracted with CH_2Cl_2 (2 × 80 ml). The combined organic phase was dried over anhydrous Na_2SO_4. The solvent was removed *in vacuo*, and the residue was purified by flash column chromatography (CH_2Cl_2) to give a pure product. White powder; yield: 4.82 g (85%). Anal. calcd for $C_{43}H_{30}N_2$ (M_r = 574.73): C, 89.86%; H, 5.26%; N, 4.87%. Found: C, 89.68%; H, 5.28%; N, 4.74%. ^{1}H NMR (500.13 MHz, $CDCl_3$), δ: 8.94 (d, $^3J_{H,H}$ = 8.0 Hz, 1H^1), 8.78 (d, $^3J_{H,H}$ = 8.3 Hz, 1H^8), 8.72 (d, $^3J_{H,H}$ = 8.3 Hz, 1H^5), 7.84 (d, $^3J_{H,H}$ = 8.3 Hz, 2H^{10}), 7.77 (t, $^3J_{H,H}$ = 7.6 Hz, 1H^7), 7.73–7.66 (m, 5H, Ar), 7.73–7.76 (m, 5H^{6,12,19}), 7.58–7.50 (m, 9H^{2,11,16,17,18}), 7.46 (d, $^3J_{H,H}$ = 8.1 Hz, 2H^9), 7.34–7.28 (m, 2H^{3,4}), 6.81 (dd, $^3J_{H,H}$ = 17.5, 10.7 Hz, 1H^{20}), 6.75 (dd, $^3J_{H,H}$ = 17.6, 10.7 Hz, 1H^{15}), 5.87 (d, $^3J_{H,H}$ = 17.5 Hz, 1H^{22}), 5.80 (d, $^3J_{H,H}$ = 17.6 Hz, 1H^{13}), 5.36 (d, $^3J_{H,H}$ = 10.9 Hz, 1H^{21}), 5.29 (d, $^3J_{H,H}$ = 10.9 Hz, 1H^{14}). ^{13}C NMR (125.76 MHz, $CDCl_3$), δ: 150.74 (N–C=N), 142.02, 140.94, 139.63, 138.75, 137.96, 137.78, 137.65, 137.07, 136.47 (*C*H=CH_2), 136.34 (*C*H=CH_2), 129.89, 129.61, 129.58, 129.44, 128.51, 128.46, 128.43, 127.47, 127.42, 127.40, 127.23, 127.08, 126.83, 126.52, 125.82, 125.10, 124.31, 123.31, 123.21, 122.96, 121.07, 114.76 (CH=*C*H_2), 114.28 (CH=*C*H_2). IR (ATR, cm^{-1}) 3082 ν (CH_{aryl}); 1630 ν ($C=C_{vinyl}$); 1608 ν (C=CN), 1495 ν (C–N) 1466 ν ($C=C_{aryl}$); 987, 907 ν (CH_{vinyl}), 831 Υ ($C–H_{aryl}$).

1,2-Bis(4-vinylphenyl)-1*H*-phenanthro[9,10-*d*]imidazole (DV-PPI) (3). **2-Br-PPI** (1) (5.0 g, 9.47 mmol), 2 M K_2CO_3 (22 ml), ethanol (50 ml), and toluene (100 ml) were combined in a three-necked flask under vigorous stirring. After the degassing, vinylboronic acid pinacol ester (3.73 ml, 21.8 mmol) and tetrakis(triphenylphosphine)palladium(0) (0.76 g, 0.654 mmol) were added. The reaction mixture was degassed with the following stirring under reflux in argon for 4 hours. TLC control (CH_2Cl_2). Then, the mixture was quenched with water (50 mL) and extracted with CH_2Cl_2 (2 × 80 ml). The combined organic phase was dried (anhydrous Na_2SO_4). The solvent was removed *in vacuo*, and the residue was purified by flash column chromatography (CH_2Cl_2) to give a pure product. White-off powder; yield: 3.2 g (80%). Anal. calcd for $C_{31}H_{22}N_2$ (M_r = 422.53): C, 88.12%; H, 5.25%; N, 6.63%. Found: C, 87.43%; H, 5.33%; N, 6.52%. ^{1}H NMR (500.13 MHz, $CDCl_3$), δ: 8.91 (dd, $^3J_{H,H}$ = 8.0 Hz, $^4J_{H,H}$ = 1.0 Hz, 1H^1), 8.76 (d, $^3J_{H,H}$ = 8.3 Hz, 1H^8), 8.70 (d, $^3J_{H,H}$ = 8.3 Hz, 1H^5), 7.76 (t, $^3J_{H,H}$ = 7.5 Hz, 1H^6), 7.65 (ddd, $^3J_{H,H}$ = 8.8, 3.3 Hz, $^4J_{H,H}$ = 1.2 Hz, 1H^7), 7.61 (d, $^3J_{H,H}$ = 8.3 Hz, 2H^{10}), 7.57 (d, $^3J_{H,H}$ = 8.3 Hz, 2H^{15}), 7.50 (ddd, $^3J_{H,H}$ = 8.5, 2.9 Hz, $^4J_{H,H}$ = 1.0 Hz, 1H^2), 7.45 (d, $^3J_{H,H}$ = 8.3 Hz, 2H^9), 7.34 (d, $^3J_{H,H}$ = 8.3 Hz, 2H^{14}), 7.28–7.26 (m, 2H^{3,4}), 6.86 (dd, $^3J_{H,H}$ = 17.6, 10.9 Hz, 1H^{16}), 6.69 (dd, $^3J_{H,H}$ = 17.6, 10.9 Hz, 1H^{11}), 5.93 (d, $^3J_{H,H}$ = 17.7 Hz, 1H^{18}), 5.77 (d, $^3J_{H,H}$ = 17.7 Hz, 1H^{13}), 5.46 (d, $^3J_{H,H}$ = 10.8 Hz, 1H^{17}), 5.28 (d, $^3J_{H,H}$ = 10.8 Hz, 1H^{12}). ^{13}C NMR (125.76 MHz, $CDCl_3$), δ: 150.75 (N–C=N), 139.00, 138.10, 137.97, 137.66, 136.35 (*C*H=CH_2), 135.79 (*C*H=CH_2), 129.93, 129.62,

Open Access Article. Published on 13 August 2025. Downloaded on 8/22/2025 11:09:28 PM. This article is licensed under a Creative Commons Attribution-NonCommercial 3.0 Unported Licence.

129.39, 129.33, 128.42, 128.32, 127.98, 127.43, 123.35, 126.48, 126.22, 125.78, 125.06, 124.26, 123.27, 123.15, 122.91, 121.04, 116.22 ($CH{=}\mathit{C}H_2$), 114.99 ($CH{=}\mathit{C}H_2$). IR (ATR, cm^{-1}) 3082 ν (CH_{aryl}); 1628 ν ($C{=}C_{vinyl}$); 1609 ν ($C{=}CN$), 1511 ν (C–N) 1452 ν ($C{=}C_{aryl}$); 982, 907 ν (CH_{vinyl}), 847 Υ ($C{-}H_{aryl}$).

Synthesis of latexes

All latex samples were prepared in a 500 ml glass reactor under a nitrogen atmosphere at the polymerization temperature of 85 °C. Distilled water (77 g), Disponil FES 993 (0.25 g), Na_2CO_3 (0.3 g), and $(NH_4)_2S_2O_8$ (0.25 g) were put into the reactor and heated to the polymerization temperature. Then the monomer emulsion consisting distilled water (150 g), Disponil FES 993 (7.5 g), Na_2CO_3 (0.7 g), of $(NH_4)_2S_2O_8$ (0.5 g), and the monomer mixture (100 g), containing completely dissolved UVA that revealed good solubility in acrylic monomers was fed into the stirred reactor during 2 h (at a feeding rate of about 2 ml min^{-1}). The polymerization reaction was then allowed to complete under the same conditions for 2 h. In this way, latexes exhibiting a solids content of about 30 wt% and pH ≈ 7 were prepared. Each latex sample was synthesized twice to verify reproducibility.

Two sets of latexes differing in the PPI derivative type, namely **DV-bPPI** and **DV-PPI**, were produced *via* the semi-continuous non-seeded emulsion polymerization technique. This procedure is known to be unique in the so-called monomer-starved conditions, which means that (i) high and immediate monomer conversion exceeding 90% is maintained during the entire progress of free-radical polymerization, and (ii) statistical copolymers of relatively homogeneous chemical composition are produced.[22] In both sets of latexes, various amounts of the respective PPI derivative (0, 0.05, 0.1, 0.25, 0.5, and 1 wt% based on the total monomer mixture) were copolymerized with standard acrylic monomers, namely, methyl methacrylate (MMA), butyl acrylate (BA), and methacrylic acid (MAA). The monomer composition of all synthesized latexes maintained a constant MMA/BA/MAA weight ratio of 43/55/2. (The ratio was adjusted to provide film formation of latex copolymers at ambient temperature. A calculated[23] T_g of the copolymer was approximately 12 °C). The latex samples were denoted as L/*X Y*, where *X* represents the PPI derivative type and *Y* reflects the percentage concentration of the respective PPI derivative in the monomer mixture. After the synthesis, the liquid latexes were characterized from the point of view of the coagulum content, monomer conversion, average hydrodynamic diameter, and zeta potential.

Preparation of latex films

Free-standing latex films of dry-film thickness of 0.6 ± 0.1 mm were prepared by pouring the latexes into silicone moulds and drying at ambient conditions (23 ± 2 °C, 50 ± 5% RH) for 30 days. The dry films were evaluated for their chemical composition using FTIR, optical properties, and UV resistance. In addition, the covalent linking of the respective PPI was verified according to the level of crosslinking of latex films expressed by the gel content and visually by monitoring the photoluminescence of the gel fraction under UV light at 365 nm using a UV lamp (Krüss Optronic, Germany).

Results and discussion

Synthesis and characterization of UV absorbers

The synthetic route to the target UVAs **DV-bPPI** (2) and **DV-PPI** (3) is depicted in Fig. 1. The intermediate **2-Br-PPI** (1) was synthesized by the Debus–Radziszewski imidazole synthesis[24] from 4-bromobenzaldehyde, phenanthrene-9,10-dione, 4-bromoaniline, and ammonium acetate in glacial acetic acid with a high yield. The purification of the intermediate was commonly performed by crystallization from EtOH and flash column chromatography (CH_2Cl_2). The targeted UVAs **DV-bPPI** (2) and **DV-PPI** (3) were synthesized by Suzuki cross-coupling reaction of the starting material **2-Br-PPI** (1) and corresponding derivatives of boronic acid, which were prepared as pure powders with yields from 80 to 85%.

The good solubility of these monomers in butyl acrylate facilitates their easy introduction into the emulsion polymerization process. All these compounds were characterized with the help of multinuclear NMR (Fig. S1–3) and IR spectroscopy (Fig. 14), while the molecular structures of (2) and (3) were determined by X-ray diffraction analysis (XRD). The structure of the synthesized intermediate **2-Br-PPI** corresponds to the literature data.[25]

^1H NMR spectrum of **DV-bPPI** revealed the characteristic signal at δ 6.75 ppm (doublet of doublets) of H^{15} proton (Fig. S2), which corresponds to the vinyl group, correlating with the *cis*-proton H^{14} (δ 5.29 ppm) and *trans*-proton H^{13} (δ 5.80 ppm). The second vinyl group is represented by the characteristic signal H^{20} at δ 6.81 ppm (doublet of doublets), as well as the *cis*-proton H^{21} (δ 5.36 ppm) and *trans*-proton H^{22} (δ 5.87 ppm) corresponding to this group. The $^{13}C\{^1H\}$ NMR spectrum also indicates a clear separation of the carbon signals of both vinyl groups, such that both CH ($CH{=}CH_2$) carbons are defined by signals at δ 136.47 and 136.34 ppm, while both CH_2 ($CH{=}$

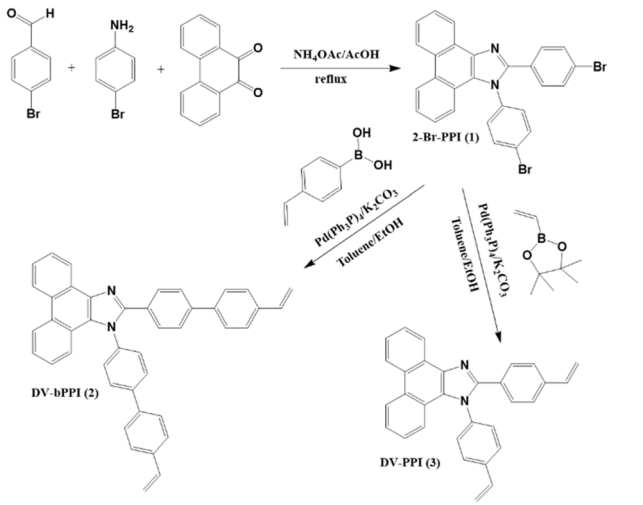

Fig. 1 Synthetic route of the target UVAs.

© 2025 The Author(s). Published by the Royal Society of Chemistry

Open Access Article. Published on 13 August 2025. Downloaded on 8/22/2025 11:09:28 PM.
This article is licensed under a Creative Commons Attribution-NonCommercial 3.0 Unported Licence.

CH_2) carbons appear as two signals at δ 114.76 and 114.28 ppm, respectively.

The vinyl groups of the **DV-PPI** monomer are represented by a characteristic signal at δ 6.69 ppm (doublet of doublets) of H^{11} proton (Fig. S3) and the corresponding signals of *cis*-H^{12} (δ 5.28 ppm) and *trans*-H^{13} (δ 5.77 ppm) protons; as well as a characteristic signal at δ 6.86 ppm (doublet of doublets) of H^{16} proton and the corresponding signals of *cis*-H^{17} (δ 5.46 ppm) and *trans*-H^{18} (δ 5.93 ppm) protons. The signals at δ 136.35 ppm and δ 135.79 ppm in the $^{13}C\{^1H\}$ NMR spectrum correspond to the CH carbons of the vinyl groups of the **DV-PPI** compound, while the CH_2 groups are determined by the signals at δ 116.22 ppm and δ 114.99 ppm.

The molecular structures of **DV-bPPI** and **DV-PPI** were determined with XRD, and they are presented in Fig. 2. XRD proved that **DV-bPPI** and **DV-PPI** are phenanthroimidazole derivatives, with the N2C3 five-membered heterocycle having well-localized single and double bonds. This can be demonstrated by bond distances C1–N2 (1.3188(15) Å in **DV-bPPI**, 1.3165(17) Å in **DV-PPI**) and C3–C2 (1.3744(16) Å in **DV-bPPI**, 1.3818(17) Å in **DV-PPI**) defining the presence of C=N and C=C bonds. In comparison, remaining C–N bonds are longer with distances C1–N1 (1.3812(19) Å in **DV-bPPI**, 1.3791(17) Å in **DV-PPI**) and C2–N2 (1.3833(16) Å in **DV-bPPI**, 1.3794(17) Å in **DV-PPI**). Aryl substituents are bonded to phenanthroimidazole by C–C and N–C single bonds with C1–C24 (1.4717(18) Å in **DV-bPPI**, 1.4722(17) Å in **DV-PPI**) and N1–C16 (1.4399(16) Å in **DV-bPPI**, 1.4368(17) Å in **DV-PPI**).

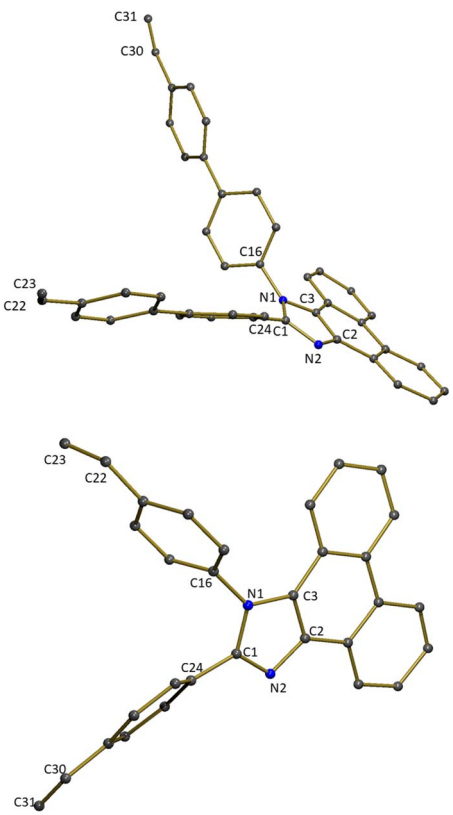

Fig. 2 Molecular structures of DV-bPPI and DV-PPI.

While the aryl substituents contain delocalized C–C bonds (distances ranging from 1.379(2) Å to 1.399(2) Å), the vinyl group contains localized C=C double bonds with the distances C30–C31 (1.317(3) Å in **DV-bPPI**, 1.320(2) Å in **DV-PPI**) and C22–C23 (1.304(3) Å in **DV-bPPI**, 1.309(2) Å in **DV-PPI**). The data, however, suggest that both vinyl groups are somewhat different within the molecule and C30–C31 bonds are slightly prolongated as compared with C22–C23.

Cyclic voltammetry (CV) of the prepared monomers **DV-bPPI** and **DV-PPI** was carried out in a 0.1 M Bu_4PF_6/CH_2Cl_2 electrolyte at a scan rate of 100 mV s^{-1} using a three-electrode electrochemical system (Ossila potentiostat), in which Pt disk (2 mm) and Pt wire were used as working and counter electrode, respectively, and Ag/Ag+ in acetonitrile as the reference electrode.[26] For both molecules, similar oxidation potential values of 1.07 (**DV-bPPI**) and 1.02 V (**DV-PPI**) (Table 1) were found, which give correspondingly similar HOMO energy levels in comparison to ferrocene. Compared to PPI (HOMO energy level −5.53 eV),[27] the HOMO energy levels of **DV-bPPI** and **DV-PPI** are similar, indicating comparable electron transfer capabilities.

The optical properties of UVAs are presented in Fig. 3. We investigated the absorbance (ABS) and photoluminescent (PL) excitation and emission features of these compounds in chloroform (0.001%) at ambient conditions, and the corresponding data are summarized in Table 1.

Both UVAs demonstrate similar absorbance spectra with the ABS maxima at 363 nm (**DV-bPPI**) and 361 nm (**DV-PPI**). The second ABS maximum around 330–345 nm can be attributed to the π–π^* transition of the substituent on the 2-imidazole position to the PPI unit.[28] The observed red shift of the absorbance maxima upon the introduction of another benzene ring at positions 2 and 9 in the phenanthroimidazole molecule indicates an increase in the conjugation length. The absorbance spectra were used for the estimation of optical band gaps (E_g) of both UVAs. The E_g values of both monomers are approximately identical (Table 1). As expected, the molar extinction coefficients 3.19×10^4 (**DV-bPPI**) and 2.64×10^4 M^{-1} cm^{-1} (**DV-PPI**), calculated from the absorbance spectra of both compounds, are close in value. The relative PL quantum yields (PL QY) of **DV-bPPI** and **DV-PPI** were investigated at ambient conditions in $CHCl_3$ to be 89 and 84%, respectively, using quinine sulfate (0.01 M H_2SO_4, PL QY = 0.54) as a standard.[29] As exemplified in Fig. 3, the PL emission spectra of **DV-bPPI** and **DV-PPI** exhibit

Table 1 Optical and electrochemical properties of UVAs

Parameters	DV-bPPI	DV-PPI
Absorbance λ_{ABS}, nm	363	361
Excitation maximum λ_{EXC}, nm	382	375
PL maximum λ_{PL}, nm	422	406
Molar extinction coefficient ε (10^4 M^{-1} cm^{-1})	3.19	2.64
Optical band gap E_g, eV	3.25	3.28
Oxidation onset potential E_{onset}, V	1.07	1.02
HOMO energy level, eV	−5.51	−5.46
LUMO energy level, eV	−2.26	−2.18
PL quantum yield PL QY, %	89	84

Open Access Article. Published on 13 August 2025. Downloaded on 8/22/2025 11:09:28 PM.
This article is licensed under a Creative Commons Attribution-NonCommercial 3.0 Unported Licence.

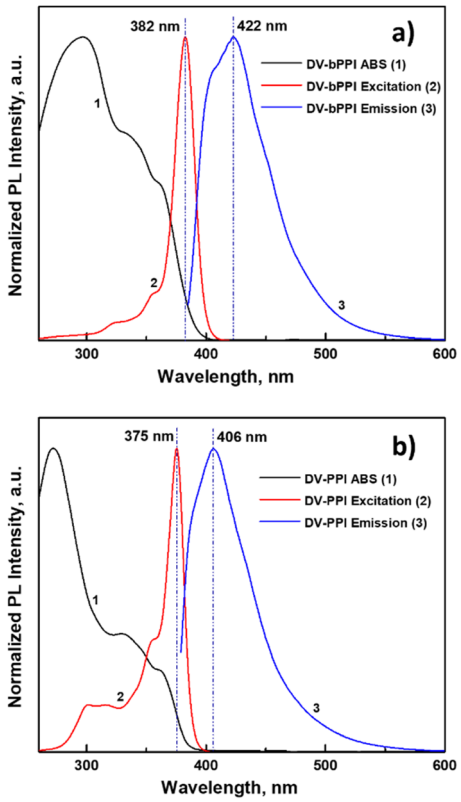

Fig. 3 Normalized absorbance (black line), excitation (red line), and emission (blue line) spectra of synthesized PPI derivatives: DV-bPPI (a) and DV-PPI (b).

broad and structureless signals with dominant maxima of 422 and 406 nm, respectively, which cover a wide range of spectrum from blue to green. Also, with the increase in molecule size, a similar red shift of the excitation spectrum is observed from 375 nm (**DV-PPI**) to 382 nm (**DV-bPPI**), with an obvious disappearance of signals in the blue region. This red shift is also explained by an increase in the chain and, accordingly, the conjugation length. Notably, both molecules exhibit slight overlaps between the absorbance, excitation, and emission spectra, thus decreasing their self-absorbance.

Properties of latexes and latex polymer films

The properties of the prepared latexes are presented in Table 2. It was found that the coagulum content (below 1.5%) and the monomer conversion (above 95%) were not influenced by the type and content of the incorporated PPI derivative. Moreover, the type and content of PPI derivative did not significantly affect the hydrodynamic diameter (ranging 80–90 nm), particle size polydispersity (below 8%), or the zeta potential (below −45 mV) of latex polymer particles. The DLS results indicate insignificant agglomeration or secondary nucleation of latex particles during the synthesis and colloidal stability of all latexes.

The optical properties of the as-prepared latex polymer films are presented in Fig. 4 and 5. Fig. 4a presents a comparative characteristic of the solution state monomer **DV-bPPI** and the solid-state latex films L/**DV-bPPI** 1% expressed in excitation and emission spectra.

We observe how the change in state, concentration, and the emergence of new bonds caused by the polymerization process led to a blue shift of the dominant excitation maxima from 382 to 361 nm and emission from 422 to 385 nm, as well as the appearance of new signals.

The unique shoulder-peak at 363 nm of **DV-bPPI**, generated by the π–π* transition of phenanthroimidazole monomer,[30] retains its position upon bonding with non-conjugated acrylates (Fig. 4b). Its intensity, as well as the presence/absence of higher energy signals, depends on the concentration of **DV-bPPI** and slightly varying film thickness. The effect of **DV-bPPI** concentration in L/**DV-bPPI** films demonstrates the appearance of saturation at the concentration of **DV-bPPI** with a maximum at 0.25% (Fig. 4c). An increase in the content of this compound likely leads to the appearance of aggregates in the polymer film mass, which represent an accumulation of unreacted monomer. However, the **DV-PPI** monomer demonstrates a steady growth in emission intensity with its increasing content in the film (Fig. 5c), suggesting its higher ability to copolymerize with acrylates in the emulsion polymerization. This monomer is also characterized by a blue shift of the excitation maxima from 375 to 361 nm and emission from 406 to 385 nm upon transition from the free dissolved form to the polymer film (Fig. 5a). We also observe retention of the position and a more pronounced signal shape of the characteristic absorbance maximum at

Table 2 Characteristics of the synthesized latexes and the gel content present in dried latex polymer films

Latex	Coagulum content, wt%	Monomer conversion, %	Hydrodynamic diameter, nm	Polydispersity index, %	Zeta potential, mV	Gel content, wt%
L 0%	0.8 ± 0.3	96.4 ± 1.0	84.7 ± 1.7	4.7 ± 4.2	−55.2 ± 2.0	73.4 ± 1.9
L/**DV-bPPI** 0.05%	1.7 ± 0.6	98.6 ± 1.2	86.4 ± 1.9	7.1 ± 3.6	−50.1 ± 2.1	72.4 ± 3.4
L/**DV-bPPI** 0.1%	0.6 ± 0.5	95.1 ± 2.1	81.3 ± 1.8	6.5 ± 3.2	−60.5 ± 1.4	71.8 ± 1.0
L/**DV-bPPI** 0.25%	0.6 ± 0.2	95.4 ± 0.9	87.1 ± 1.8	6.6 ± 0.5	−47.0 ± 1.5	73.3 ± 1.8
L/**DV-bPPI** 0.5%	0.8 ± 0.1	95.6 ± 1.1	87.2 ± 0.7	8.1 ± 2.5	−51.4 ± 2.3	70.8 ± 0.7
L/**DV-bPPI** 1%	1.2 ± 0.4	97.4 ± 1.4	87.1 ± 0.7	6.6 ± 3.5	−46.9 ± 1.8	69.2 ± 1.5
L/**DV-PPI** 0.05%	0.4 ± 0.2	95.4 ± 0.7	86.5 ± 1.3	6.7 ± 3.0	−50.2 ± 1.5	70.0 ± 2.6
L/**DV-PPI** 0.1%	0.7 ± 0.2	97.7 ± 1.5	80.5 ± 1.9	5.2 ± 2.2	−48.1 ± 1.3	77.8 ± 2.6
L/**DV-PPI** 0.25%	1.2 ± 0.3	95.0 ± 1.0	88.6 ± 0.9	7.8 ± 3.0	−57.1 ± 1.6	77.9 ± 1.4
L/**DV-PPI** 0.5%	1.5 ± 0.4	96.6 ± 0.8	82.8 ± 1.3	7.6 ± 3.3	−50.7 ± 2.2	78.4 ± 4.5
L/**DV-PPI** 1%	0.9 ± 0.4	95.8 ± 1.3	82.0 ± 0.4	7.7 ± 1.6	−52.3 ± 0.7	78.9 ± 2.5

© 2025 The Author(s). Published by the Royal Society of Chemistry

Open Access Article. Published on 13 August 2025. Downloaded on 8/22/2025 11:09:28 PM.
This article is licensed under a Creative Commons Attribution-NonCommercial 3.0 Unported Licence.

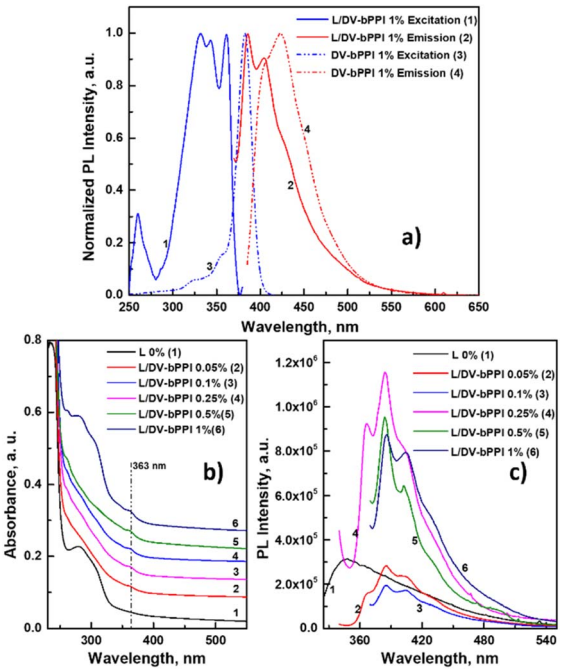

Fig. 4 Excitation and emission spectra of the L/**DV-bPPI** 1% polymer film (solid lines) in comparison with excitation and emission spectra of the PPI derivative (dashed lines) (a); absorbance spectra of L/**DV-bPPI** films with different **DV-bPPI** content (b); PL spectra of L/**DV-bPPI** films with different **DV-bPPI** content (c). Unless otherwise noted, solid lines represent spectra of polymer films and dashed lines represent spectra of corresponding monomers in solution.

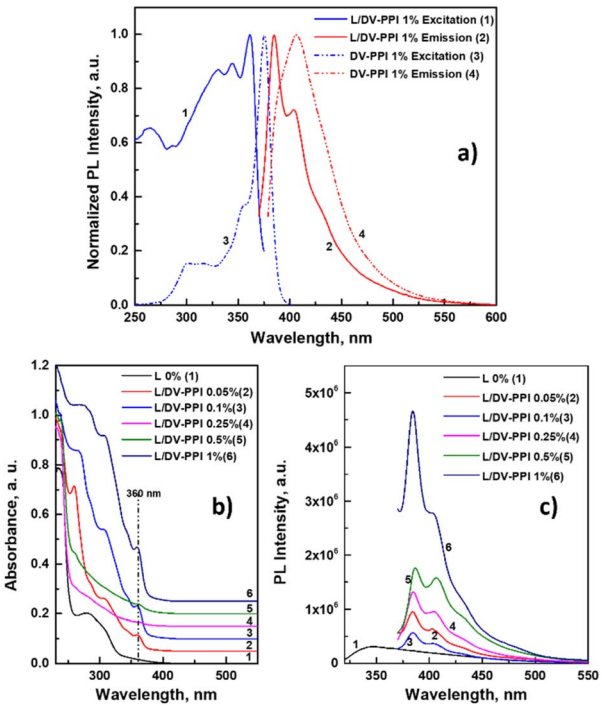

Fig. 5 Excitation and emission spectra of the L/**DV-PPI** 1% film (solid lines) in comparison with excitation and emission spectra of pure monomer (dashed lines) (a); absorbance spectra of L/**DV-PPI** films with different emissive monomer content (b); PL spectra of L/**DV-PPI** films with different emissive monomer content (c). Unless otherwise noted, solid lines represent spectra of polymer films and dashed lines represent spectra of corresponding monomers in solution.

360 nm. It should be noted that the ability of both monomers to copolymerize with acrylates under the presented conditions differs, which is confirmed by the results obtained using other techniques.

The observed blue shift of emission and excitation maxima in polymer films, compared to the monomer solution, suggests a rigidification of the molecular environment and reduced conformational freedom upon covalent incorporation into the crosslinked polymer matrix. This restriction likely suppresses non-radiative relaxation pathways, contributing to the high PL QY values observed in gel fractions. No clear signs of self-quenching or Förster-type energy transfer were detected up to 0.5 wt% concentration, particularly for **DV-PPI**, suggesting that the distance between emissive units remains sufficiently large and aggregation is minimal. This behavior indicates that the photoluminescent mechanism in the solid-state remains dominated by local π–π^* transitions, with limited intermolecular interactions. Potential quenching *via* polar sites or water is further minimized due to the hydrophobic backbone of the latex matrix. The copolymerization ability, *i.e.*, the covalent linking of PPI derivatives in polymer chains, was assessed according to the level of crosslinking expressed by the gel content (Table 2). It was assumed that the PPI derivative molecule (bearing two vinyl functionalities) could be linked to the polymer backbone *via* the free-radical polymerization of double bonds in vinyl groups, forming a linear polymer chain in the case where one vinyl group is involved in the polymerization or a crosslinked polymer network in the case where both vinyl groups are reacted. A considerably high gel content (around 75 wt%) was found for all polymer types including the reference polymer L 0%, which is probably a consequence of the presence of ionic bonds between cations (multivalent or even monovalent) present in latex aqueous environment and ionized carboxyl groups on polymer backbone that had been formed due to saponification of acrylate or methacrylate ester side groups during polymerization performed in alkaline environment.[31] The increase in gel content with the increasing concentration of the introduced PPI derivative was found only for the series L/**DV-PPI**, which suggests not only its covalent anchoring to polymer chains but also a weak crosslinking activity.

To indirectly verify the covalent linking, a simple experiment based on irradiating the polymer gel fraction (obtained by Soxhlet extraction) with UV light of a wavelength of 365 nm (Fig. 6) showed stronger photoluminescence (blue light emission) in the case of polymer gels from latexes L/**DV-bPPI** 1% and L/**DV-PPI** 1% in contrast to weak blue light emission of the polymer gel from the latex L 0%. This phenomenon denies the sole physical entrapment of the PPI derivatives in the latex polymer matrix and indicates at least their partial covalent linking to polymer chains.

© 2025 The Author(s). Published by the Royal Society of Chemistry

Open Access Article. Published on 13 August 2025. Downloaded on 8/22/2025 11:09:28 PM.
This article is licensed under a Creative Commons Attribution-NonCommercial 3.0 Unported Licence.

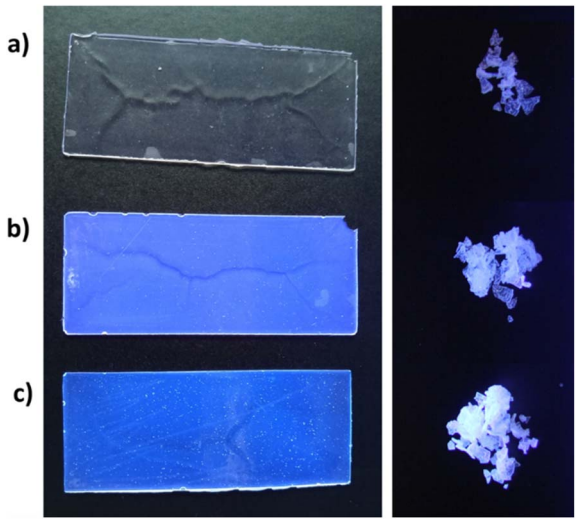

Fig. 6 Photographs of dry latex polymer films and the corresponding gel fractions (obtained after Soxhlet extraction in THF) irradiated by UV light of a wavelength of 365 nm: L 0% (a), L/**DV-bPPI** 1% (b), L/**DV-PPI** 1% (c).

UV resistance of latex polymer films

The UV resistance of latex films was assessed visually (observing macroscopic and microscopic appearance of polymer films), and according to changes in selected characteristics between the non-exposed and UV-exposed films, namely, the chemical structure using FTIR, T_g measured using DSC, and thermo-mechanical properties determined by DMA. The UV-stabilizing efficiency of the incorporated PPI derivatives in the latex polymer matrix was assessed according to changes in selected characteristics between the non-exposed and UV-exposed polymer films, namely, the chemical structure using FTIR, T_g, and thermo-mechanical properties determined by DMA. In addition to these exact methods, a visual assessment of the differences between the non-exposed and UV-exposed films was performed using optical microscopy.

In Fig. 7, the reference latex film (L 0%) is displayed before and after the UV irradiation. The UV irradiation led to the cracking and overall embrittlement of the latex film, which broke into irregularly shaped fragments with sizes between 1–10 mm. This phenomenon is a manifestation of chain scission reactions.[32] The introduction of the PPI derivatives into the latex film structure led to significantly different outcomes, depending on the type of PPI derivative. For the L/**DV-bPPI** series (Fig. 8), dark-yellowish spots occurred in both the non-exposed and the UV-irradiated films at high **DV-bPPI** concentration (see Fig. 8e and f). Here, two explanations come to mind. The first idea revolves around the possibly lower water solubility of the **DV-bPPI** compound (compared to standard acrylic monomers and **DV-PPI**), which would lead to easier (faster) transport of the standard acrylic monomers from emulsified monomer droplets into the water phase in comparison with **DV-bPPI**. Consequently, the surplus amount of **DV-bPPI** would be concentrated within the diminishing monomer droplets, forming small reservoirs that would later, during the latex film drying phase, further merge as the larger pockets between the latex polymer particles, as the interdiffusion and coalescence of the latex film occur. The second (more probable) idea then considers (instead of the largely lower solubility) a significantly lower reactivity of **DV-bPPI** in comparison with acrylic monomers and **DV-PPI**.

The latter claim is derived from weak polarization of both vinylic groups of **DV-bPPI** (the influence of the imidazole ring is partially shielded by the insertion of the additional benzene rings on the path to the vinylic bonds). As such, the **DV-bPPI** present (dissolved) in the water phase would not react with free radicals in the continuous water phase, therefore not being part of oligomeric radicals that are essential for the entry to monomer-swollen micelles (which is followed by propagation reaction with monomers therein). According to the observations

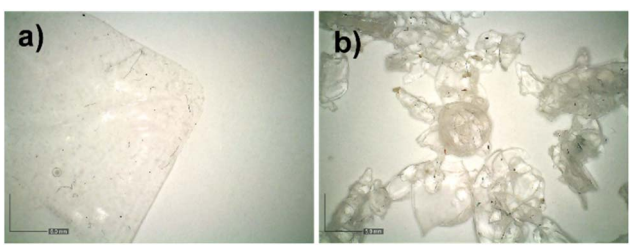

Fig. 7 Macroscopic appearance of the reference latex polymer film L 0% before (a) and after (b) the UV irradiation. The scale bars indicate 5 mm.

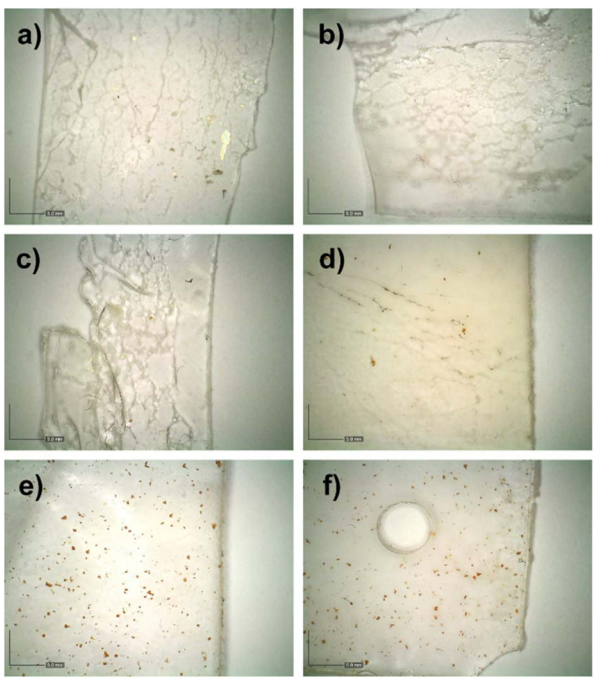

Fig. 8 Macroscopic appearance of the latex polymer films containing **DV-bPPI** derivative at different concentrations: L/**DV-bPPI** 0.05% exposed to UV irradiation (a), L/**DV-bPPI** 0.1% exposed to UV irradiation (b), L/**DV-bPPI** 0.25% exposed to UV irradiation (c), L/**DV-bPPI** 0.5% (d), L/**DV-bPPI** 1% exposed to UV irradiation (e), L/**DV-bPPI** 1% non-exposed (f). The scale bars indicate 5 mm.

© 2025 The Author(s). Published by the Royal Society of Chemistry

Open Access Article. Published on 13 August 2025. Downloaded on 8/22/2025 11:09:28 PM. This article is licensed under a Creative Commons Attribution-NonCommercial 3.0 Unported Licence.

demonstrated in Fig. 6, we can also assume that a small portion of **DV-bPPI** molecules diffused into the monomer-swollen micelles statistically, on their own. The residual **DV-bPPI** derivative remaining in the water phase then, again, got concentrated within the pockets formed during the latex film drying. Interestingly, some sort of **DV-bPPI** derivative solubility or reactivity saturation appears to occur, since the integral amount of the non-polymerized **DV-bPPI** concentrated within the pockets disproportionally increased with its initial concentration in the monomer mixture; very few unreacted **DV-bPPI** pockets were present in the L/**DV-bPPI** 0.5% latex film, whereas pronouncedly larger **DV-bPPI** pockets occurred in the L/**DV-bPPI** 1% latex film. The number or magnitude of these reservoirs did not change by the UV irradiation of the latex films (compare Fig. 8e and f). The UV-stabilizing effect of the **DV-bPPI** derivative is then demonstrated by the development of cracks in the UV-irradiated latex films with decreasing **DV-bPPI** concentration. Whereas the film with 1 wt% of **DV-bPPI** was practically indistinguishable before and after the UV irradiation, the decreasing concentration of the **DV-bPPI** led to the formation of cracks on the surface as well as within the latex film (clearly visible at **DV-bPPI** concentrations $\leq$0.25 wt%), and to the overall film embrittlement (similar to that of the reference latex film L 0% – see Fig. 7b).

The macroscopic appearance of the latex films comprising the **DV-PPI** compound is shown in Fig. 9. In contrast to the **DV-bPPI**, no reservoirs with concentrated **DV-PPI** derivative were visible even for the highest **DV-PPI** concentration, which indicates its increased solubility and/or reactivity and incorporation into latex polymer particles. In addition, the protective ability of **DV-PPI** against UV irradiation appears to be higher compared to **DV-bPPI**. Already at 0.1 wt% of incorporated **DV-PPI**, the amount of the UV-induced cracks in the latex film was largely reduced, and for the concentrations 0.25 and 0.5 wt%, the latex films seemed to be defect-free even after the intense UV irradiation. However, the further increasing concentration of **DV-PPI** to 1 wt% resulted in the embrittlement of the UV-irradiated latex film (Fig. 9).

This seemingly counterintuitive finding will be further explored and explained in the following paragraphs. Similar findings were also observed at the micro-scale, using the regular optical microscopy (Fig. 10–12). The micrographs obtained at

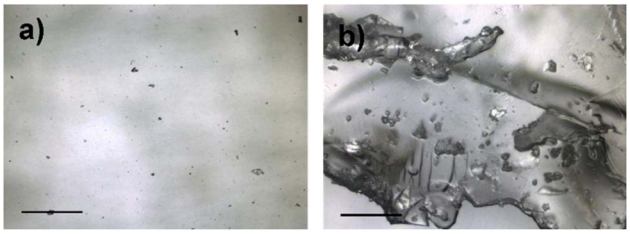

Fig. 10 Micrographs obtained for the reference latex film L 0% before (a) and after (b) the UV irradiation. The scale bars indicate 200 μm.

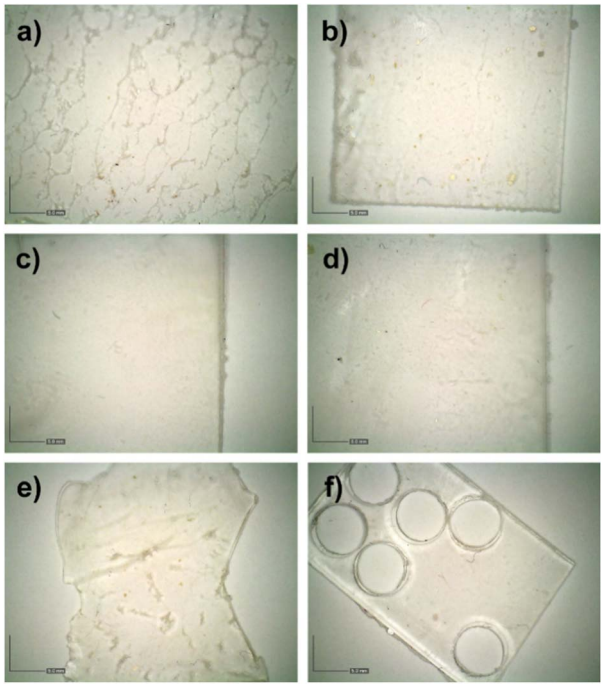

Fig. 9 Macroscopic appearance of the latex polymer films containing **DV-PPI** derivative at different concentrations: L/**DV-PPI** 0.05% exposed to UV irradiation (a), L/**DV-PPI** 0.1% exposed to UV irradiation (b), L/**DV-PPI** 0.25% exposed to UV irradiation (c), L/**DV-PPI** 0.5% (d), L/**DV-PPI** 1% exposed to UV irradiation (e), L/**DV-PPI** 1% non-exposed (f). The scale bars indicate 5 mm.

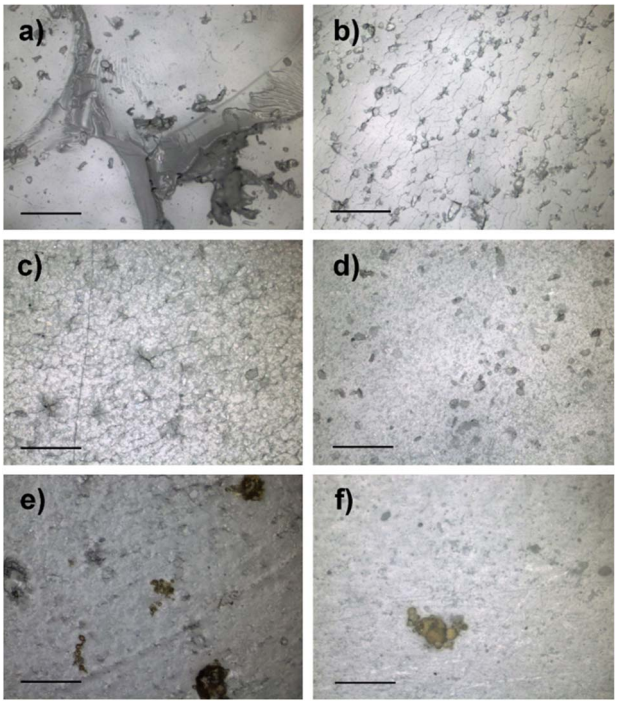

Fig. 11 Micrographs for the latex films containing **DV-bPPI** derivative at different concentrations: L/**DV-bPPI** 0.05% exposed to UV irradiation (a), L/**DV-bPPI** 0.1% exposed to UV irradiation (b), L/**DV-bPPI** 0.25% exposed to UV irradiation (c), L/**DV-bPPI** 0.5% (d), L/**DV-bPPI** 1% exposed to UV irradiation (e), L/**DV-bPPI** 1% non-exposed (f). The scale bars indicate 200 μm.

Open Access Article. Published on 13 August 2025. Downloaded on 8/22/2025 11:09:28 PM.
This article is licensed under a Creative Commons Attribution-NonCommercial 3.0 Unported Licence.

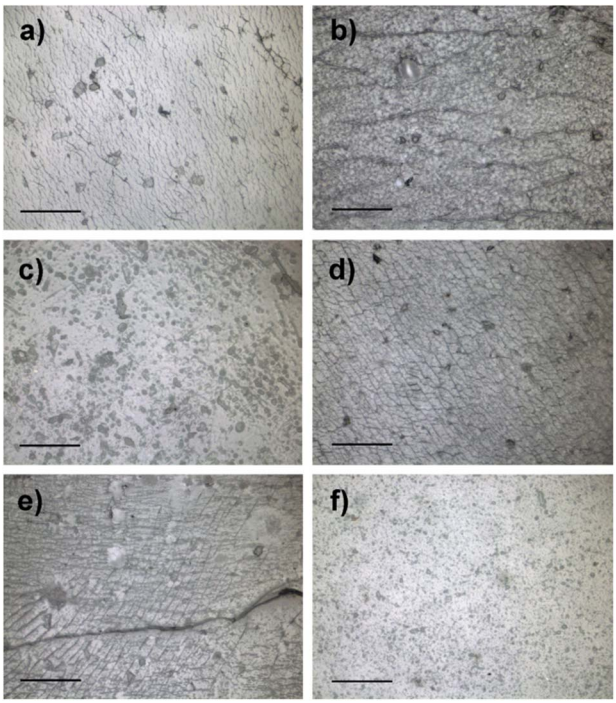

Fig. 12 Micrographs for the latex films containing **DV-PPI** derivative at different concentrations: L/**DV-PPI** 0.05% exposed to UV irradiation (a), L/**DV-PPI** 0.1% exposed to UV irradiation (b), L/**DV-PPI** 0.25% exposed to UV irradiation (c), L/**DV-PPI** 0.5% (d), L/**DV-PPI** 1% exposed to UV irradiation (e), L/**DV-PPI** 1% non-exposed (f). The scale bars indicate 200 μm.

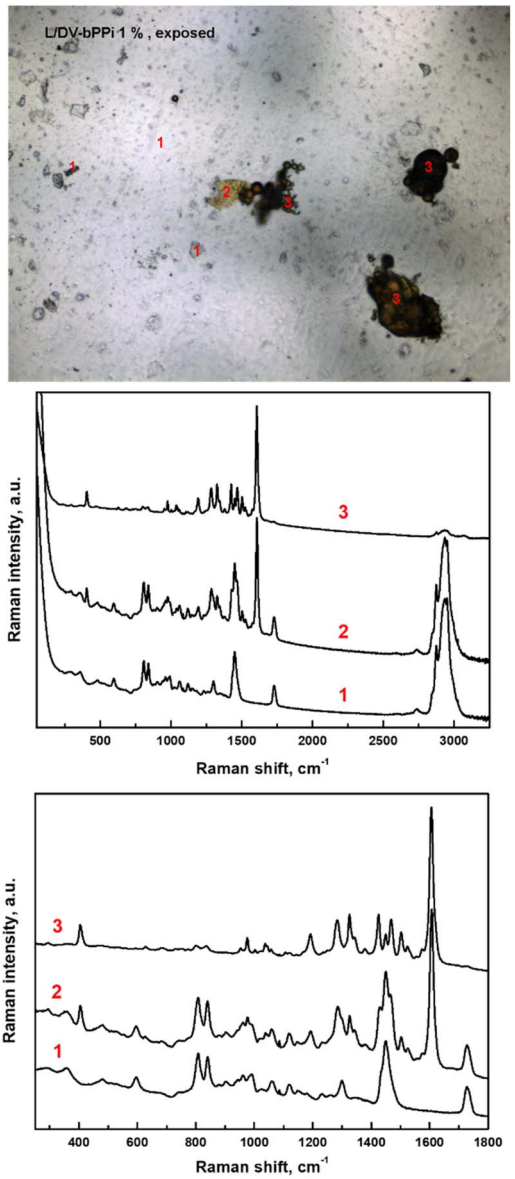

Fig. 13 Representative micrograph obtained for L/**DV-bPPI** 1% latex film exposed to UV irradiation; the numbers 1–3 denote various morphological features. Features denoted with no. 1 include all types of defects commonly observed for all non-exposed and exposed L/DV films. The Raman spectra (depicted in full scale as well as zoomed-in on the region of main bands) then correspond in their denotation to the archetypal features depicted in the micrograph.

larger magnification show that for the UV-exposed L/**DV-bPPI** series of latex films, the cracks visible on the micro-scale disappeared for the **DV-bPPI** concentrations ≥0.5 wt%, which is practically consistent with the lower magnification observations. On the other hand, for the UV-exposed L/**DV-PPI** series of latex films, the crack-free film was observed only for the **DV-PPI** concentration of 0.25 wt% (contrary to the ∼0.1–0.5 wt% range estimated based on the lower magnitude observations). This indicates that the micro-scale observations appear to be necessary for the accurate evaluation of the UV-stabilizing efficiency. Nonetheless, the basic evaluation of the UV-stabilizing effect can be correctly estimated even using the naked eye or low-magnification optics.

In a complementary manner to optical microscopy, Raman microscopy was used to identify the structural/chemical morphology of the non-exposed as well as the UV-exposed latex films. In Fig. 13, the three archetypal Raman spectra corresponding to the different morphological features of the studied latex polymer films are depicted. Apart from the L/**DV-bPPI** films with high **DV-bPPI** concentrations (0.5 and 1 wt%), all types of defects observed in the case of all studied films (Fig. 10–12) exhibited exactly similar signal of the pure latex polymer matrix. This fact suggests that the PPI derivative was covalently incorporated into the latex polymeric structure (losing its characteristic Raman bands) or that it was homogeneously spread across the whole latex polymer matrix, with the information about its exact location and/or bonding not being accessible due to its concentration being below the instrumental detection limit. The only exceptions were the films L/**DV-bPPI** 0.5% and L/**DV-bPPI** 1% (the latter being depicted in Fig. 13 as an example), where the macroscopic pockets with practically pure **DV-bPPI** occurred. This was confirmed by Raman measurements, which showed that the large orange-to-black defects indeed gave the signal of pure **DV-bPPI.** Note that the actual diameter of the sphere, from which the Raman spectrum is collected, is ∼10–20 μm (progressively more focused toward the centre); hence, the parasitic weak residual signal from the surrounding latex matrix can occur in the

© 2025 The Author(s). Published by the Royal Society of Chemistry

Open Access Article. Published on 13 August 2025. Downloaded on 8/22/2025 11:09:28 PM. This article is licensed under a Creative Commons Attribution-NonCommercial 3.0 Unported Licence.

spectrum focused just on the **DV-bPPI** pocket. In addition to the pure **DV-bPPI** pockets (locations marked with "3" in Fig. 13), an occasional light-yellow spot was found in the close vicinity of the pockets, where the **DV-bPPI** was mixed within the latex matrix in very high concentration (location marked with "2" in Fig. 13). In such a case, the corresponding Raman spectrum was a sum of both pure Raman signals, *i.e.*, of the pure latex and pure UVA.

The IR spectra of the **DV-bPPI** and **DV-PPI** monomers, as well as the freshly prepared and irradiated L/**DV-bPPI** and L/**DV-PPI** latexes, are demonstrated in Fig. 14. The IR spectrum of the **DV-bPPI** compound (Fig. 14a) presents signals at 3082 cm^{-1} corresponding to the C–H stretching vibration at the aromatic ring, as well as the spectrum of the **DV-PPI** monomer (Fig. 14b).

The characteristic bands of the vinyl group[33] at 1630 cm^{-1} for the **DV-bPPI** monomer and 1628 cm^{-1} for **DV-PPI** are assigned to the $CH{=}CH_2$ stretching vibrations. The presence of the imidazole ring in the structure of the monomers is confirmed by the signals at 1608, 1495, and 1466 cm^{-1}, which can be attributed to the C–N, C=C, and C=N stretching bands of substituted imidazole.[34] The weak band around the 1050–1100 cm^{-1} region can be ascribed to the out-of-plane bending vibrations of the aromatic ring. The peaks in the region from 830 to 990 cm^{-1} are assigned to the stretching vibrations of C–H bonds in conjugated molecules.

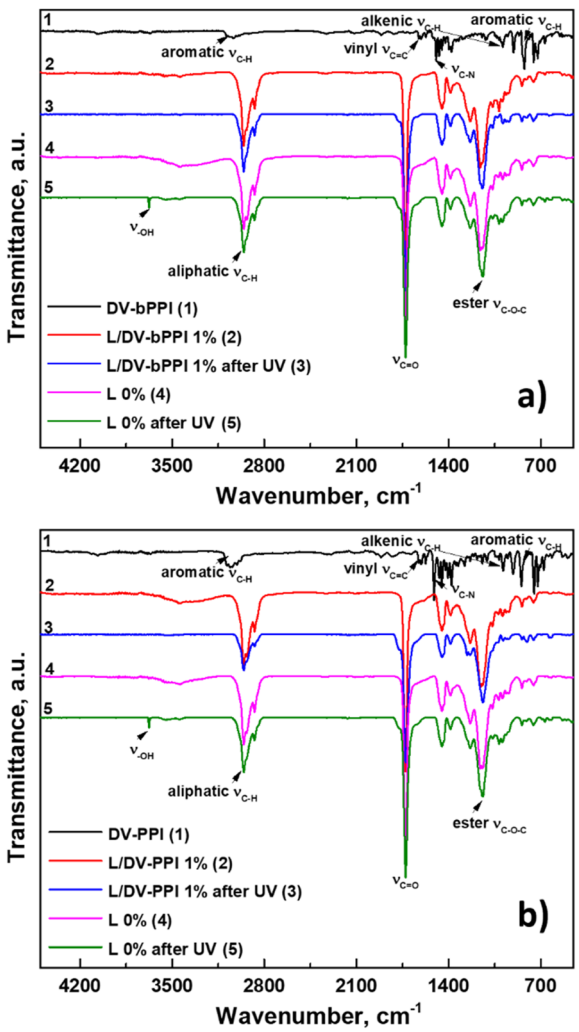

Fig. 14 FTIR spectra of monomers (UVAs), unexposed and UV-exposed latexes: DV-bPPI (a); DV-PPI (b).

The molecular structure of the latex films is characterized by the presence of vibrations in the region of 2870–2960 cm^{-1}, corresponding to vibrations of aliphatic groups. It could be seen that intensive peaks (curves 2,4 in Fig. 14a and b) at 1728 cm^{-1} and 1138 cm^{-1}, ascribed as stretching vibration peaks of C=O and C–O–C bonds in the ester group, are similar for all latex spectra, including the spectrum of UV-exposed polymers. The characteristic stretching peaks (both latexes) at 1453 cm^{-1} and 1381 cm^{-1} are attributed to $-OCH_3$ groups in MMA, and 987 cm^{-1}, 842 cm^{-1}, and 756 cm^{-1} are attributed to –OBu groups in BA.[3] The appearance of a hydroxyl group (3676 cm^{-1}) in free latex L 0% after UV irradiation confirms UV-induced oxidation resulting in alcohol groups. As follows from the spectra of both exposed latexes comprising PPI derivatives (curves 3 in Fig. 14a and b), irradiation with UV light did not reveal significant changes in the intensity and position of characteristic signals. Thus, it can be assumed that both PPI derivatives in a concentration of 1 wt% protected acrylic polymer chains from significant photodegradation at the molecular level.

The thermal behaviour of the UV-irradiated latex films containing different amounts of the PPI derivatives was investigated using DSC. In particular, the measurements of the films' behaviour in the glass transition range (Fig. 15) have shown that the UV irradiation of the reference latex film significantly increased its T_g by approx. 4 °C. This is most probably the consequence of an additional UV-induced oxidative crosslinking of polyacrylate chains containing butyl ester groups, which are known to undergo fast and extensive photo-oxidative crosslinking.[35,36] In both series of latex polymers, the presence of the respective PPI derivative appeared (at least partially, depending on the PPI derivative concentration) to prevent this effect. A clear change of T_g (prevention of its increase) is apparent in the case of L/**DV-bPPI** films; more stochastic but still certainly significant prevention of the T_g increase occurred also for the L/**DV-PPI** films.

The original DMA measurements were performed in the −30–40 °C temperature range. Whereas the soft non-exposed latex A crucial set of findings was provided employing DMA. The evaluation of the mechanical properties of the UV-irradiated films was expressed in terms of the storage modulus (E'), loss modulus (E''), and loss factor (tan δ) (Fig. 16). Films exhibited a typical viscoelastic response to the applied compression under the dynamic load, the UV-irradiated latex film samples were more brittle, which resulted in a high level of signal noise below T_g, and clamping-effect-induced data-distortion above T_g (due to the combination of the higher dynamic force limit and UV-reduced film thickness), see Fig. S4 in SI for an example. Note that this is a common phenomenon in the case of the temperature-resolved DMA penetration measurements, which, however, were the only applicable DMA mode due to the surface corrugation and very small dimensions

Open Access Article. Published on 13 August 2025. Downloaded on 8/22/2025 11:09:28 PM.
This article is licensed under a Creative Commons Attribution-NonCommercial 3.0 Unported Licence.

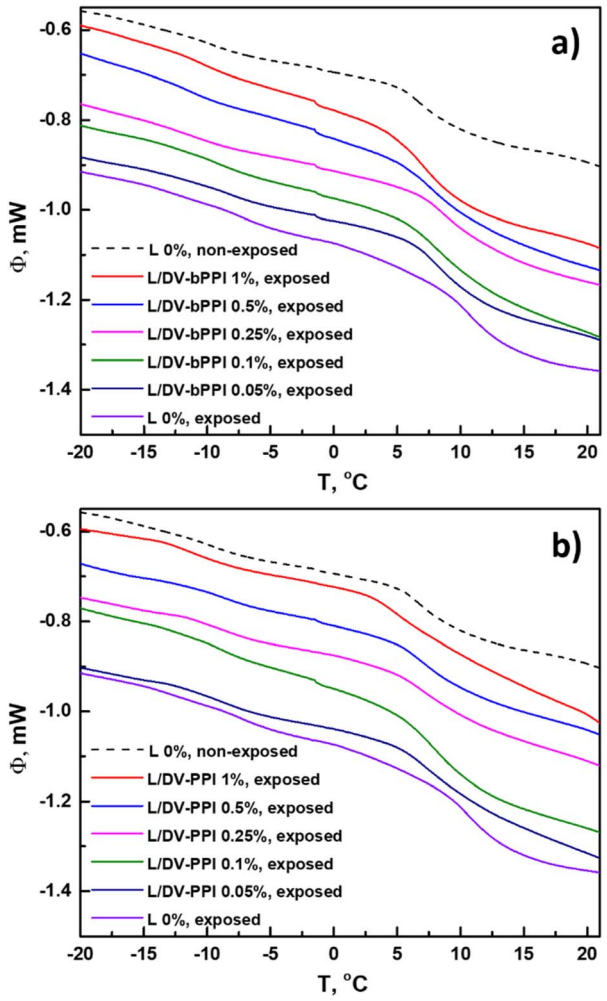

Fig. 15 DSC curves measured in the glass transition range for the latex films exposed to UV irradiation in contrast to the non-exposed reference latex film L 0%: L/**DV-bPPI** series (a); L/**DV-PPI** series (b).

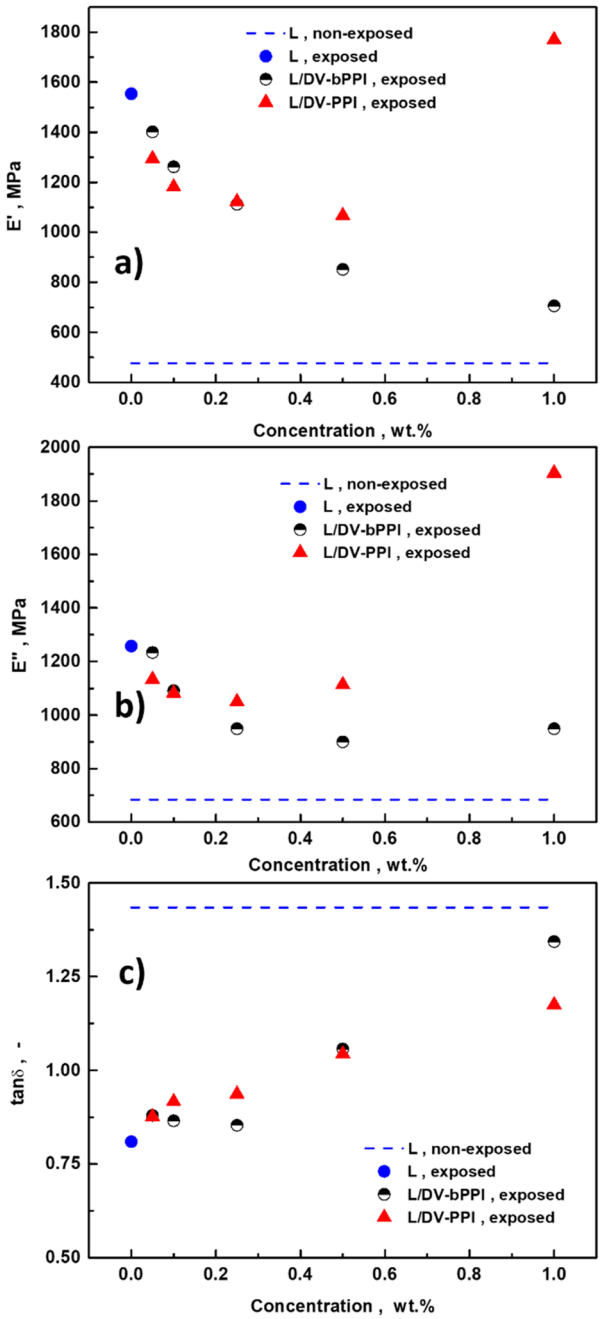

Fig. 16 Mechanical properties evaluated using DMA for the latex films exposed to UV irradiation, in contrast to the non-exposed reference latex film L 0%: (a) storage modulus (E'), (b) loss modulus (E''), (c) loss factor (tan δ).

of certain samples being intact after the UV irradiation. For this reason, only a rather narrow temperature range was usable for the reliable and comparable determination of the viscoelastic characteristics of all latex films. For the present comparisons, the mechanical properties were evaluated at 10 °C (~ middle of the glass transition range), see Fig. 16. Starting with E', which is an indicative parameter of the elastic energy stored in the material and represents the material's stiffness and solid-like behaviour, the UV-irradiation enhanced the elasticity in the case of all latex films, which was manifested as multifold increase of E'. As the elastic element is rooted in entanglements that make the material resist deformation and return to its original shape, this phenomenon is probably related to photo-oxidative crosslinking. Specifically, for the reference latex film L 0%, the ratio of $E'_{\text{exposed}}/E'_{\text{non-exposed}}$ was approximately 3. The increasing concentration of the **DV-bPPI** led to a continuous decrease of the UV-irradiation-induced elasticity (reaching $E'_{\text{exposed}}/E'_{\text{non-exposed}} \approx 1.4$ at 1 wt% of **DV-bPPI**), indicating its pronounced UV-stabilizing effect. On the contrary, the increasing concentration of **DV-PPI** in the polymer matrix manifested through a non-monotonous trend in the E'-concentration dependence. In particular, the initially pronounced steep decrease of E' with the initial **DV-PPI** addition (up to 0.1 wt%) rapidly ceased with further increasing **DV-PPI** concentration, and the decrease of E' practically stopped at ~0.5 wt% of **DV-PPI** in the latex matrix. Moreover, at 1 wt% of **DV-PPI**, E' increased above the level of the reference UV-irradiated film L 0% containing no PPI derivative. This

© 2025 The Author(s). Published by the Royal Society of Chemistry

Open Access Article. Published on 13 August 2025. Downloaded on 8/22/2025 11:09:28 PM.
This article is licensed under a Creative Commons Attribution-NonCommercial 3.0 Unported Licence.

phenomenon will be more thoroughly examined in our next studies.

Qualitatively similar but even more pronounced (magnitude-wise) influence of the PPI derivatives' concentration was found for E'', which is an indicative parameter of the dissipated energy lost in the cyclic strain and represents the liquid-like behaviour. The UV-irradiation enhanced the viscous element (rooted in chain flow) in the case of all latex films, probably because of scission reactions. Regarding the **DV-bPPI**, its increasing concentration led to a continuous decrease of the UV-irradiation-induced plasticity, revealing again its significant UV-stabilizing effect.

In the case of the **DV-PPI**, a non-monotonous trend in the E''–concentration dependence appeared again. It is noteworthy that the increase of E'' with increasing PPI derivative concentration occurred already for 0.5 wt% of **DV-PPI**, and, even more importantly, a slight increase of E'' was observed also for **DV-bPPI** at 1 wt%. This indicates that the UV-induced scission reactions of the polymer matrix occurred to a greater extent at higher concentrations of both PPI derivatives. The combination of scission reactions and macromolecular coupling *via* oxidative crosslinking is most probably responsible for the macroscopic defects and structural inhomogeneities observed in the corresponding micrographs in Fig. 8 and 9.

The last evaluated quantity describing the mechanical behaviour and viscoelasticity of the UV-irradiated films was the loss factor tan δ, which expresses the internal mechanical losses or damping and can be a significant measure of material impact strength and toughness. In the case of polymers, the loss factor also provides a measure of the balance between the elastic and viscous phases in a polymeric structure and is associated with molecular movements and chain flexibility. The evolution of this quantity, which monotonously and practically linearly changes for both incorporated PPI derivatives between the values characterizing the exposed and non-exposed reference latex film L 0%, clearly confirms the strong and roughly similar stabilizing efficiency of the novel PPI derivatives in protection against the UV irradiation.

Conclusions

This study aimed to develop and evaluate novel UV-absorbing phenanthroimidazole (PPI) derivatives, **DV-bPPI** and **DV-PPI**, as covalently incorporated stabilizers in waterborne all-acrylic latex coatings. The overarching objective was to improve the UV resistance of these coatings through the chemical anchoring of PPI-based UV absorbers (UVAs), enabling long-term photostability while maintaining transparency and mechanical integrity at lower UVA concentrations.

Both vinyl-functionalized PPI derivatives were successfully synthesized *via* Suzuki cross-coupling reactions and characterized using NMR, FTIR, and X-ray diffraction analyses. Their covalent incorporation into the polymer matrix through emulsion polymerization was confirmed by gel content analysis and emission of the gel fractions, suggesting successful chemical anchoring of the UVA moieties. The presence of the PPI derivatives substantially mitigated the effects of UV-induced degradation, as evidenced by spectroscopic (FTIR, Raman), thermal (DSC), and mechanical (DMA) analyses. Importantly, both derivatives protected the polymer structure against oxidative crosslinking and chain scission, leading to improved retention of thermal and viscoelastic properties after UV exposure.

Comparative analysis revealed that **DV-PPI** exhibited superior integration and stabilizing efficiency at lower concentrations (0.25–0.5 wt%), attributed to its higher solubility and reactivity. In contrast, **DV-bPPI** showed effective UV stabilization primarily at higher loadings (≥0.5 wt%) but suffered from solubility/reactivity limitations, leading to the formation of unreacted aggregates within the film matrix. These disparities highlight the influence of molecular structure on copolymerization behaviour and UV-stabilizing performance.

Overall, this work demonstrates the feasibility of covalently binding photoluminescent PPI derivatives into acrylic latex films to achieve efficient UV stabilization. **DV-PPI**, in particular, emerges as a promising low-concentration additive for high-performance, photostable waterborne coatings, offering a chemically robust and optically clear alternative to conventional UVAs.

Author contributions

L. L. and J. M. conceptualized the research and designed the methodology; L. L. performed the UVAs syntheses; J. M. conducted the polymer synthesis experiments; Z. R. determined molecular structure of UVAs; L. L., R. J., M. V., and J. H. performed the UVAs characterization studies and analysed the data; R. S., J. H., and M. K. performed the polymer characterization studies and analysed the data; L. L., J. M, R. S., and R. J. wrote the manuscript. All authors edited and approved the manuscript. M. V., J. M., and R. J. acquired the funding. J. M. supervised the work.

Conflicts of interest

There are no conflicts to declare.

Data availability

Data for the crystal structure reported in this paper have been deposited at the Cambridge Crystallographic Data Centre (CCDC) under the deposition numbers 2414305 (for **DV-bPPI**) and 2414306 (for **DV-PPI**). The datasets generated during and/or analysed during the current study are available in the Figshare repository, DOI: **https://www.doi.org/10.6084/m9.figshare.29423225**.

CCDC 2414305 and 2414306 contain the supplementary crystallographic data for this paper.[37,38]

^{1}H and ^{13}C NMR spectra of the synthesized compounds are also provided in the SI. See DOI: **https://doi.org/10.1039/d5ra05109f**.

Open Access Article. Published on 13 August 2025. Downloaded on 8/22/2025 11:09:28 PM. This article is licensed under a Creative Commons Attribution-NonCommercial 3.0 Unported Licence.

Acknowledgements

Authors appreciate the financial support from the project "Innovative materials with high added value suitable for applications – INMA (CZ.02.01.01/00/23_021/0008593), support from the grant LM2023037 from the Ministry of Education, Youth and Sports of the Czech Republic.

References

1 J. Deng, B. Chen, X. Luo and W. Yang, *Macromolecules*, 2009, **42**, 933–941, DOI: 10.1021/ma8026468.
2 C. S. Chern, *Prog. Polym. Sci.*, 2006, **31**, 443–486, DOI: 10.1016/j.progpolymsci.2006.02.001.
3 W. Dong, L. Zhou, Y. Guo, Y. Tang, R. Pan, M. Liu and D. He, *J. Coat. Technol. Res.*, 2022, **19**, 607–617, DOI: 10.1007/s11998-021-00550-5.
4 J. Machotova, H. Zgoni, S. Podzimek, R. Svoboda, J. Palarcik and J. Snuparek, *Prog. Org. Coat.*, 2017, **111**, 258–268, DOI: 10.1016/j.porgcoat.2017.06.004.
5 M. Aguirre, M. Paulis and J. R. Leiza, *J. Mater. Chem. A*, 2013, **1**, 3155–3164, DOI: 10.1039/c2ta00762b.
6 J. Miklecic, S. L. Blagojevic, M. Petric and V. Jirous-Rajkovic, *Prog. Org. Coat.*, 2015, **89**, 67–73, DOI: 10.1016/j.porgcoat.2015.07.016.
7 R. Iyengar and B. Schellenberg, *Polym. Degrad. Stab.*, 1998, **61**, 151–159, DOI: 10.1016/S0141-3910(97)00144-4.
8 K. Mikame, Y. Ohashi, Y. Naito, H. Nishimura, M. Katahira, S. Sugawara, K. Koike and T. Watanabe, *ACS Sustainable Chem. Eng.*, 2021, **9**, 16651–16658, DOI: 10.1021/acssuschemeng.1c05415.
9 C. Decker and K. Zahouily, *J. Polym. Sci. Part A Polym. Chem.*, 1998, **36**, 2571–2577, DOI: 10.1002/(SICI)1099-0518(199810)36:14<2571::AID-POLA16>3.0.CO;2-F.
10 P. Katangur, P. K. Patra and S. B. Warner, *Polym. Degrad. Stab.*, 2006, **91**, 2437–2443, DOI: 10.1016/j.polymdegradstab.2006.03.018.
11 N. Li, Y. Chen, Y. Bao, Z. Zhang, Z. Wu and Z. Chen, *Appl. Surf. Sci.*, 2015, **332**, 186–192, DOI: 10.1016/j.apsusc.2015.01.112.
12 V. V. Rajan, R. Waber and J. Wieser, *J. Appl. Polym. Sci.*, 2012, **124**, 4007–4014, DOI: 10.1002/app.34560.
13 Z. Liu, S. Chen and J. Zhang, *J. Appl. Polym. Sci.*, 2013, **127**, 1135–1143, DOI: 10.1002/app.37955.
14 C. Liu, Z. Li, T. J. Hajagos, D. Kishpaugh, D. Y. Chen and Q. Pei, *ACS Nano*, 2017, **11**, 6422–6429, DOI: 10.1021/acsnano.7b02923.
15 Y. Zhang, K.-L. Zhang, J. Liu, J.-H. Wang, Y.-Q. Feng, P.-J. Deng, X. Tian, G. Han and D. Li, *J. Mater. Chem. C*, 2021, **9**, 10226–10234, DOI: 10.1039/D1TC01928G.
16 Y. Zhang, J.-H. Wang, G. Han, F. Lu and Q.-X. Tong, *RSC Adv.*, 2016, **6**, 70800–70806, DOI: 10.1039/C6RA13605B.
17 H. Goudarzi, D. Habibi and A. Monem, *RSC Adv.*, 2024, **14**, 22459–22468, DOI: 10.1039/D4RA03302G.
18 I. Singh, R. Rani, V. Luxami and K. Paul, *Eur. J. Med. Chem.*, 2019, **166**, 267–278, DOI: 10.1016/j.ejmech.2019.01.053.
19 Y. Yuan, D. Li, X. Zhang, X. Zhao, Y. Liu, J. Zhang and Y. Wang, *New J. Chem.*, 2011, **35**, 1534–1540, DOI: 10.1039/C1NJ20072K.
20 N. Cliff, M. Kanouni, C. Peters, P. V. Yaneff and K. Adamsons, *J. Coat. Technol. Res.*, 2005, **2**, 371–376, DOI: 10.1007/s11998-005-0005-y.
21 H. Ling and L. Junyan, *J. Fluorine Chem.*, 2008, **129**, 590–594, DOI: 10.1016/j.jfluchem.2008.04.007.
22 J. Ugelstad, M. S. El-Aasser and J. W. Vanderhoff, *J. Polym. Sci.*, 1973, **11**(8), 503–516, DOI: 10.1002/pol.1973.130110803.
23 T. G. Fox Jr and P. J. Flory, *J. Appl. Phys.*, 1950, **21**, 581–591, DOI: 10.1063/1.1699711.
24 W. Qin, Z. Yang, Y. Jiang, J. W. Y. Lam, G. Liang, H. S. Kwok Ben and Z. Tang, *Chem. Mater.*, 2015, **27**, 3892–3900, DOI: 10.1021/acs.chemmater.5b00568.
25 Z. Wang, P. Lu, S. Chen, Z. Gao, F. Shen, W. Zhang, Y. Xu, H. S. Kwok and Y. Ma, *J. Mater. Chem.*, 2011, **21**, 5451–5458, DOI: 10.1039/C1JM10321K.
26 H. Jin, X. Li, T. Tan, S. Wang, Y. Xiao and J. Tian, *Dyes Pigm.*, 2014, **106**, 154–162, DOI: 10.1016/j.dyepig.2014.02.018.
27 A. I. Solomatina, K. M. Kuznetsov, V. V. Gurzhiy, V. V. Pavlovskiy, V. V. Porsev, R. A. Evarestov and S. P. Tunik, *Dalton Trans.*, 2020, **49**, 6751–6764, DOI: 10.1039/D0DT00568A.
28 Z. Gao, Z. Wang, T. Shan, Y. Liu, F. Shen, Y. Pan, H. Zhang, X. He, P. Lu, B. Yang and Y. Ma, *Org. Electron.*, 2014, **15**, 2667–2675, DOI: 10.1016/j.orgel.2014.07.019.
29 J. W. Eastman, *Photochem. Photobiol.*, 1967, **6**, 55–62, DOI: 10.1111/j.1751-1097.1967.tb08790.x.
30 Y. Jia, S. Wu, Y. Zhang, S. Fan, X. Zhao, H. Liu, X. Dong, S. Wang and X. Li, *Org. Electron.*, 2019, **69**, 289–296, DOI: 10.1016/j.orgel.2019.03.044.
31 N. T. Vuong and N. A. Hiep, *Vietnam J. Chem.*, 2016, **54**(2), 249–255, DOI: 10.15625/0866-7144.2016-00270; https://vjs.ac.vn/vjchem/article/view/0866-7144.2016-00270.
32 B. Ranby, *J. Macromol. Sci., Part A*, 1993, **30**, 583–600, DOI: 10.1080/10601329308021247.
33 B. I. Cherifi, M. Belbachir and A. Rahmouni, *Discover Chem. Eng.*, 2021, **1**, 5, DOI: 10.1007/s43938-021-00005-8.
34 N. Lu, H. Liu, R. Huang, Y. Gu, X. Yan, T. Zhang, Z. Xu, H. Xu, Y. Xing, Y. Song, X. Li and Z. Zhang, *Anal. Chem.*, 2019, **91**(18), 11938–11946, DOI: 10.1021/acs.analchem.9b02746.
35 O. Chiantore, L. Trossarelli and M. Lazzari, *Polymer*, 2000, **41**(5), 1657–1667, DOI: 10.1016/S0032-3861(99)00349-3.
36 O. Chiantore and M. Lazzari, *Polymer*, 2001, **42**(1), 17–27, DOI: 10.1016/S0032-3861(00)00327-X.
37 L. Loghina, J. Machotova, R. Svoboda, J. Houdek, M. Kohl, Z. Ruzickova, R. Jambor and M. Vlcek, CCDC 2414305: Photoluminescent phenanthroimidazole derivatives as covalently linked UV stabilizers for latex coatings, 2025, DOI: 10.5517/ccdc.csd.cc2m18ts.
38 L. Loghina, J. Machotova, R. Svoboda, J. Houdek, M. Kohl, Z. Ruzickova, R. Jambor and M. Vlcek, CCDC 2414306: Photoluminescent phenanthroimidazole derivatives as covalently linked UV stabilizers for latex coatings, 2025, DOI: 10.5517/ccdc.csd.cc2m18vt.

© 2025 The Author(s). Published by the Royal Society of Chemistry